Association Dynamics in Solutions of Hairy-Rod Polymers

G. Petekidis,† D. Vlassopoulos,* G. Fytas, and N. Kountourakis

Foundation for Research & Technology−Hellas, Institute of Electronic Structure & Laser, P.O. Box 1527, 71110 Heraklion, Crete, Greece

S. Kumar

Pennsylvania State University, Department of Materials Science and Engineering, 320 Steidle Building, University Park, Pennsylvania 16802-5007

Received September 13, 1996; Revised Manuscript Received December 12, 1996[⊗]

ABSTRACT: Photon correlation spectroscopy in the polarized (VV) and depolarized (VH) geometries has been utilized in order to investigate the aggregation dynamics in toluene solutions of a hairy-rod polymer, poly(*p*-phenylene) with flexible dodecyl side chains. Static and dynamic results from the dilute regime suggest that polymer molecules form small aggregates, typically trimers, even at very low concentrations. In the semidilute regime, results at different scattering wavevectors (q) in both the VV and VH geometry reveal two new relaxation processes (slow and ultra slow), in addition to the faster cooperative diffusion and reorientation of the trimers, respectively. They are attributed to the formation of large anisotropic clusters (of typical size 570 nm), with inherent crystallization, as revealed by X-ray scattering. After about 2 weeks the clusters settle under the action of gravity and form an opaque sediment. Assessment of the aggregation modes has been carried out by sediment redispersion. The first stages of this process, which exhibit multiple scattering, reveal a steeper than exponential relaxation, associated with a sedimentation-induced velocity gradient in a transient pseudonetwork formed by the dispersed clusters. In the single scattering limit, reached at later stages, the two relaxation processes are related to reorientation (slow) and number density fluctuation (ultraslow) of the anisotropic clusters. On the basis of simple thermodynamic arguments, we argue that rodlike macromolecules exhibit a larger activation energy barrier compared to their flexible counterparts, in agreement with the experimental evidence.

I. Introduction

Rigid-rod polymers are materials of substantial scientific and technological interest due to the wide range of astonishing properties they exhibit; these are mainly the isotropic−nematic and other transitions, the anisotropic diffusion, and the strong coupling between translational and rotational diffusion.[1] The underlying factor behind these properties is their anisotropic shape, which is of course characteristic of the rodlike architecture, in contrast to the more common flexible polymers. In addition, and in contrast to the most widely studied rigid-rod polymers (such as poly(γ-benzyl L-glutamate), hydroxypropylcellulose, denaturated DNA, and tobacco virus), poly(*p*-phenylene)-based polymers exhibit significant inherent optical polarizability anisotropy; this property can provide valuable information concerning the reorientational dynamics,[2] as well as the conformation of the macromolecules in solution.[3] Strong molecular anisotropy is necessary for the measurement of the above mentioned distinct physical properties of rigid-rod polymers, by utilizing static and dynamic depolarized light scattering, which is an extremely sensitive probe of collective orientation fluctuations, and thus structural changes or transitions, even at a molecular scale. Of particular importance is the coupling of orientational to translational degrees of freedom, since it is related to the complicated interactions of these rigid macromolecules, especially at high concentrations.[1,2,4] In fact, in such systems it is desired to control the balance between attractive and repulsive dispersive forces in order to be able to measure truly molecular properties (avoiding interference with aggregation phenomena). Typically, the attractive forces (of the van der Waals type) are short-ranged, and rods attract each other preferentially in the parallel configuration.[4]

On the practical side, it is not possible to obtain highly concentrated isotropic solutions of hairy-rod molecules, due to solubility limits, despite the fact that the side chains were introduced to improve solubility;[5] further, dynamic light scattering investigations reveal the occurrence of aggregation, manifested as an extra slow relaxation process.[6−9] Moreover, macroscopic observations of areas of opaqueness, accompanied by increased dichroism[10] with time at high concentrations, support the aggregation picture. All this evidence points to the important role of attractive interactions in the physical properties of concentrated solutions of hairy rods and underlines the need to fundamentally understand the association of these materials. The latter, which is precisely the scope of the present paper, can be accomplished through a systematic investigation of the dynamics of both concentration and orientation fluctuations at various concentrations above the overlap concentration, as a function of temperature and time.

In addition to the important considerations presented above, it is necessary to stress the great potential of hairy-rod polymers for technological applications; in particular, these materials exhibit nonlinear optical properties and can be used as films in the photonics and electronics industry.[11] In this respect, it is essential to control these properties, in terms of their relationship to their molecular and microsctructural characteristics, and thus a full-scale characterization (both in solution and in the melt) is imperative.

In this paper we present a thorough investigation of the association dynamics in dilute and concentrated solutions of a poly(*p*-phenylene) with flexible dodecyl side chains, and its relationship to cluster sedimentation, as a function of temperature and time. In the remainder of this paper, the following aspects are covered: Section II presents a concise review of the

* Corresponding author.
† Also at Physics Department, University of Crete, Heraklion 71110, Crete, Greece.
⊗ Abstract published in *Advance ACS Abstracts,* February 1, 1997.

S0024-9297(96)01366-6 CCC: $14.00

relevant aggregation phenomena, with an emphasis on the open questions in the field of hairy-rod polymers. Section III represents a detailed description of the systems used and the experimental procedure followed. The results are presented and discussed in view of the various physical parameters in section IV. Finally, section V summarizes the main conclusions of this work.

II. Main Features of Aggregation Processes and the Challenge for Rigid Rods

The association of molecular or larger entities represents a very broad scientific field, that has been studied extensively for almost a century. Most of the work to date deals with the behavior of colloidal dispersions, and significant advances have been made in recent years due to developments in both experimental instrumentation and theoretical concepts. Setting aside the flocculation induced by electrostatic forces,[12] or kinematics,[13] aggregation in a stabilized colloidal dispersion is a function of the volume fraction of the suspended particles.[14−16] Initially, single colloidal particles undergo Brownian motion until small clusters are formed (with increasing concentration); then cluster and particle diffusion results in formation of larger aggregates, and so on. The key factor controlling the formation of aggregate structures is the balance among short-range interparticle forces.[1,4] The process of cluster growth, when irreversible, has a fractal structure and is characterized by two limiting modes, depending on whether the sticking probability is about 1 or much smaller than 1.[17]

Directly related to the aggregation problem is the sedimentation of colloidal particles. This process is controlled by the combined action of the Brownian motion and gravity. The coupling between these two driving forces gives rise to a rich variety of physical phenomena, ranging from cluster formation to cluster deposition and settling of a gelled suspension.[12,18] Furthermore, the sedimentation of aggregates can induce further aggregation, controlled by the convective transport of the aggregating material.[19] Thus, in order to understand the mechanism and dynamics of aggregation under these circumstances, it is imperative to control the coupling between cluster diffusion time and cluster settling time.[18,20]

Dynamic light scattering represents a powerful tool for the investigation of the aggregation process, since it provides information on the aggregation dynamics and size of association of the various moieties through a combination of scattered intensity and relaxation rate measurements.[21,22] Moreover, depending on the system investigated, the measurement of depolarized, in addition to the polarized light scattering, is essential because of its sensitivity and unique information on the structure and shape of the aggregates.[23−25]

It has been known for several years that rodlike polymers in solution aggregate in various solvents.[6,26] The physical grounds of this process are not clearly understood yet, but it seems that the balance of interparticle forces results in a dominance of van der Waals attractions, leading to aggregation. It is recognized, however, that the nature of interparticle forces cannot be easily determined for solutions of anisotropic particles, since electrostatic and hard-core forces act on the particles positions and orientations in a different way; typically, with increasing concentration hard-core repulsion induces a nematic order of the particles, whereas uniformly charged rods tend toward a perpendicular orientation.[1,4] There is clear evidence that aggregation can be observed in fresh solutions (within 24 h from preparation), but the kinetics of this process is characterized by much longer times.[27] Phenomenology suggests that a simple mass-action model[28] can describe the main features of aggregation in terms of cluster formation (dimers and higher-order associations), as shown recently in the case of poly(*p*-phenylene terephthalamide) solutions.[29] However, it cannot explain the origin of aggregation. The probable relevance of the aggregation of rigid polymers to their phase behavior, and in particular to transitions such as gelation, crystallization, or isotropic−nematic, is one of the central questions in this field. In this direction, recent work[30] on the phase separation of poly(γ-benzyl L-glutamate) in benzyl alcohol, suggests that gelation is due to a combination of crystallization and phase separation via spinodal decomposition. Although molecular aggregation is not explicitly discussed, it is clearly implied that this process is indeed associated with the mechanism of gelation; it is interesting to note in that respect, that two modes of aggregation are considered, namely the binary associations resulting in small clusters, and the associations of the latter into larger aggregates.[30,31]

Chart 1. Hairy-Rod Poly(*p*-phenylene) with Dodecyl Side Chains

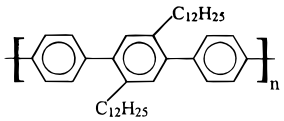

An attempt to put together the ideas from colloidal aggregation and dynamic light scattering from semidilute solutions of side-chain liquid crystalline polymers was presented in ref 9. These workers observed cluster formation at a critical concentration independent of the molecular weight, and suggested that it is due to attractive interactions. Clusters were very large and with nonfractal structure, whereas no evidence of long-range liquid crystalline order inside these aggregates was found, from static depolarized light scattering. Similar findings were also reported on the behavior of concentrated colloidal suspensions of anisotropic poly(isobutene)-grafted boehmite rods, using static and dynamic light scattering.[32] At high volume fractions they found an extra relaxation process, attributed to the presence of clusters.

In our opinion the following crucial questions remain open: (i) the deeper understanding of the origin and mechanism of aggregation; (ii) the ordering of the molecules and the characteristic size and shape of the aggregate structures; (iii) the kinetics of aggregation and its relation to sedimentation, which usually accompanies this process; and (iv) the potential relevance of macromolecular self-assembly to polymer−solvent phase separation or transitions such as gelation or isotropic−nematic. These questions will be addressed in the rest of this paper, with the aim to provide some insight into the complex problem of self-assembly in rigid-rod polymers.

III. Experimental Section

Materials. The synthesis of a series of hairy-rod poly(*p*-phenylenes), abbreviated as PPP, with dodecyl side chains (the hairs) has been reported elsewhere.[33] In the present work a PPP (Chart 1) with number-average molecular weight M_n = 9900 was used. The M_n was determined by membrane osmometry and the polydispersity was estimated to be $M_w/M_n \approx 3$, based on static light scattering measurements in a mixed cyclohexane/chloroform solvent, at 25 °C. The number-average contour length was L_n = 257 Å. Thus, the onset of the semidilute region is c* (=$1/L^3$) ≈ 0.11% by weight, and that of

the concentrated region c^{**} ($=1/dL^2$, d being the average diameter of the molecule) is 5.7% by weight if we take $d = 5$ Å, and 1.7% if we take $d = 17$ Å (in the latter case we take into account the side chains as well[2]). In the present study, we have investigated both dilute and semidilute PPP solutions in toluene, with concentrations in the range 0.1%−0.4% and 3.5%−5%, respectively. Solutions were prepared by dissolving the appropriate amount of PPP in spectroscopic grade toluene under continuous strong stirring for about 24 h. Dust-free samples were subsequently obtained by careful filtration through a 0.22 μm Teflon Millipore filter into a dust-free light scattering cell (o.d. 12.5 mm).

Photon Correlation Spectroscopy (PCS). The autocorrelation function of the polarized or depolarized light scattering intensity, $G(q,t) = \langle I(q,t)\, I(q,0)\rangle/\langle |I(q,0)|\rangle^2$, with $I(q,0)$ the mean light scattering intensity at a wavevector q ($I_{VV}(q,0)$ for the polarized geometry and $I_{VH}(q,0)$ for the depolarized geometry), was measured at different scattering angles, θ, mainly with an automated ALV goniometer and an ALV-5000 full digital correlator (320 channels) over the time range $10^{-7}-10^3$ s. The light source was a Nd:YAG dye-pumped air-cooled laser (Adlas DRY 325) with a single mode intensity of 160 mW and $\lambda =$ 532 nm. For experiments at temperatures above 50 °C, a homemade fixed-angle PCS setup was used in conjunction with the ALV-5000 correlator. It uses an Ar^+ laser light source, at 300 mW single mode and wavelength $\lambda = 488$ nm, and measures intensity autocorrelation functions simultaneously (using a fiber optics probe) at two scattering angles, namely 45 and 135°. At a given value of the scattering wavevector, $q = (4\pi n/\lambda)\sin(\theta/2)$, where n is the refractive index of the medium, the measured homodyne normalized light scattering intensity autocorrelation function $G(q,t)$ is given by the Siegert relation:[34]

$$G(q,t) = [1 + f^*|\alpha\, C(q,t)|^2] \tag{1}$$

where f^* is an experimental instrument factor calculated by means of a standard, α is the fraction of the total scattered intensity arising from fluctuations (with correlation times above 0.1 μs), and $C(q,t)$ is the normalized field correlation function:

$$C(q,t) = \frac{\langle E(q,0)\, E(q,t)\rangle}{\langle |E(q,0)|^2\rangle} \tag{2}$$

where $E(q,t)$ represents the scattered electric field at scattering wavevector q and time t. Before each measurement, the test samples were always left to equilibrate for at least 1 h (unless measurements were carried out in the transient settling regime, as discussed below). During the measurement the intensity of the scattered laser light remained constant. Whenever possible, the analysis of the experimental correlation functions, $C(q,t)$, was carried out by performing their inverse Laplace transform (ILT), using the program CONTIN.[35] This method assumes that $C(q,t)$ is represented by a superposition of exponentials:

$$\alpha C(q,t) = \int_{-\infty}^{\infty} L(\ln \tau)\, \exp(-t/\tau)\, \mathrm{d}(\ln \tau) \tag{3}$$

which describe a continuous spectrum of relaxation times $L(\ln\tau)$; the latter is used to determine the average characteristic relaxation times, τ. In some cases involving relaxation processes decaying faster than single exponential, the ILT analysis was not adequate, and the correlation functions were represented by the Kohlrausch−Williams−Watts (KWW) function:

$$C(q,t) = \exp[(-t/\tau)^{\beta}] \tag{4}$$

where β is the shape parameter (usually $0 \le \beta \le 1$, with $\beta = 1$ corresponding to a single exponential relaxation mode; the rare case $\beta > 1$ is associated with steeper than single exponential decays).

Static Light Scattering. The ALV automated setup used for PCS was employed for the static measurements as well. The range of angles scanned was 15−150°.

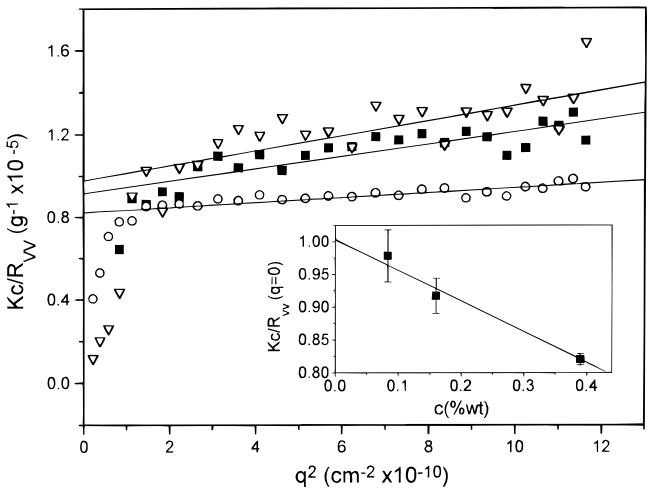

Figure 1. Polarized (VV) static light scattering results for PPP in toluene at 25 °C and various concentrations: (○) 0.39% by weight; (■) 0.16%; (▽) 0.084%. Solid lines represent fits to the high-wavevector (q) region. Inset: Determination of molecular weight by extrapolation of Kc/R_{VV} at $q = 0$ (■), at infinite dilution (solid line).

X-ray Scattering. X-ray diffraction patterns of various PPP sediment samples were recorded with a curved position-sensitive detector (INEL-CPS 120) using a Guinier focusing camera equipped with a bent quartz monochromator (Cu Kα_1). PPP powder was measured with a Rigaku D/max-2400 diffractometer, equipped with a graphite monochromator, utilizing a 12 kW rotating anode X-ray generator (Cu Kα_1).

Experimental Protocol. The studies carried out are divided in two main parts: (a) dilute regime and (b) semidilute regime. In the former case, the key question is whether one can measure truly molecular transport properties. In the latter case, the main concern is the understanding of the mechanism, nature, and kinetics of association, as well as the effects of temperature and sedimentation on the experimental correlation functions. In each case the experimental tool was a combination of static and dynamic (PCS) light scattering, performed on equilibrated systems at various concentrations, temperatures, scattering angles, and settling regimes.

IV. Results and Discussion

A. Dilute Regime. Static and dynamic light scattering measurements were carried out in dilute solutions (concentration range 0.07%−0.39% by weight), at various temperatures, and in two different solvents (toluene and chloroform).

(i) Statics. Static light scattering measurements were carried out in toluene, at concentrations 0.084%, 0.159%, and 0.39% by weight (corresponding to a c/c^* range from 0.8 to 4.4, respectively), and temperatures 25, 50, and 80 °C. The purpose of these measurements was to estimate the second virial coefficient A_2 and hence the solvent quality. The data revealed a weak q dependence of the intensity at scattering angles above 30°, whereas at lower angles an enhanced intensity was observed. Due to the careful way of collecting static data (the trace of the scattered intensity remained constant, without any fluctuations whatsoever), the presence of dust can be excluded as a potential cause of the observed excess intensity at low angles. This sharp intensity deviation at low q's is normally attributed to aggregation[36] and has been reported in several other systems.[8,32]

For all concentrations tested, the VV intensity at $q = 0$ ($I_{VV}(0)$), obtained from the $I_{VV}(q)^{-1}$ versus q^2 plot (a typical plot is depicted in Figure 1, at 25 °C), increases as the temperature decreases. A smaller change is found at lower concentrations. It should be noted that

the extrapolation at $q = 0$ for I_{VV} was always done using the data from scattering angles above 30°, due to the significant scattering at low angles. It is also noted that in contrast to I_{VV}, I_{VH} does not exhibit an upturn at low q's. This behavior can be rationalized as the existence of a few isotropic clusters, even at low concentrations. A_2 was estimated from the dependence of Kc/R_{VV} on q^2, where K is a constant containing the refractive index n and refractive index increment dn/dc, c is the concentration of the polymer, and R_{VV} is the Rayleigh factor, computed from the known R_{VV} of the solvent toluene. A_2 was found to be negative at all temperatures investigated, with a nearly unchanged value of -5×10^{-4} cm^2/g. This result suggests that the solvent quality is not good, and the system will eventually phase separate and aggregate under these solvent conditions.

In addition to A_2, static measurements revealed that the z-average radius of gyration, $(R_g)_z$, was 220 Å. Using the formula[37] (for a rod of diameter 17 Å)

$$(R_g^2)_z = \frac{(m+2)(m+3)}{(m+1)^2}\frac{L_w^2}{12} + \frac{d^2}{8} \qquad (5)$$

where m is the polydispersity index ($m = (M_w/M_n - 1)^{-1}$), the weight-average contour length L_w was found to vary from 385 to 440 Å, when m varies from 0.5 to 1. It is noted that from eq 5 d appears insensitive to the calculation of L_w. Furthermore, the weight-average molecular weight M_w was determined from extrapolation of Kc/R_{VV} at infinite dilution (inset of Figure 1), yielding $M_w \approx 100\,000$ at 25 °C, $M_w \approx 74\,000$ at 50 °C, and $M_w \approx 52\,500$ at 80 °C. In chloroform at 20 °C and $c = 0.07\%$, $M_w \approx 36\,900$. These results seem to be in disagreement with those reported in a mixed solvent of cyclohexane and chloroform, where it was found that at 25 °C, $M_w \approx 29\,700$,[33] and support the idea that rods are probably aggregated into small units, probably trimers or tetramers under these conditions. We shall term these small aggregates as trimers (typical size) in the rest of the paper. Based on the above numbers, the degree of aggregation amounts to 3.3 for a solution in toluene at 25 °C. Setting aside the slight difference in temperature, which cannot account for the observed deviation, the clear message is that PPP tends to associate in toluene. If the semiflexible conformation of the polymer chains is taken into account (using the wormlike model), the radius of gyration is given by[37]

$$(R_g^2)_z = \frac{(m+2)}{3(m+1)} l L_w - l^2 + \frac{2l^3}{L_w}\left(1 - \frac{l}{m(m+1)}\left[\left(\frac{(m+1)}{L_w}\right)^2 - \frac{\left(\frac{m+1}{L_w}\right)^{m+2}}{\left(\frac{m+1}{L_w} + \frac{1}{l}\right)^m}\right]\right) \qquad (6)$$

From this equation, for a value of the persistence length l between 150 and 220 Å, L_w varies between 740 and 500 Å, leading to similar results as in the rigid-rod case; it is noted that given the polydispersity, the L_w estimated from ref 33 is 770 Å.

(ii) Dynamics. PCS measurements were carried out in the same dilute solutions in toluene and chloroform, and in the temperature range 10−50 °C, yielding a single relaxation process (translational diffusion). Before use, each solution was heated at a high temperature (about 80 °C), where it was checked that one relaxation process was present; it was subsequently cooled to the test temperature and left to equilibrate for 1 h. Measurements were repeated at several times, during a period of 1 year, and indicated the same single relaxation process unchanged. This represents a direct demonstration of the time stability of the solution investigated. At this low concentration, the VH dynamics associated with the rotational diffusion of PPP is faster than 10^{-6} s and thus falls outside the time window of the correlator, as inferred from the flat correlation functions.

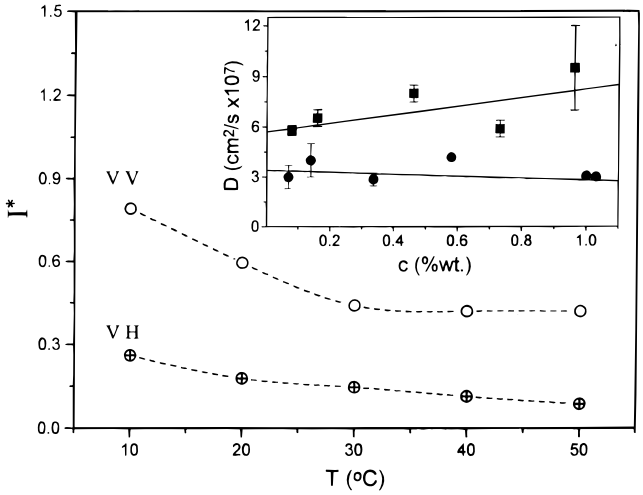

Figure 2. Total scattering intensities I^* for polarized (VV) and depolarized (VH) PCS measurements, extrapolated at $q = 0$, for the 0.21% by weight PPP/toluene solution, as a function of temperature. Both intensities are normalized to the VV intensity of toluene. Lines are drawn to guide the eye. Inset: Translation diffusion coefficients at various concentrations of PPP/toluene (●) and PPP/chloroform (■) for determination of diffusion at infinite dilution D_0. Solid lines represent best fits.

Figure 2 depicts the corresponding VV and VH scattered intensities due to the polymer (normalized to the corresponding VV intensity of toluene), at $q = 0$. An unexpected increase of both intensities as the temperature drops is clearly observed. $I_{VV}(0)$ and $I_{VH}(0)$ exhibit a 90% and 180% increase, respectively, as the temperature is decreased from 50 to 10 °C. In contrast, I_{VH} remained q-independent in the scattering angle range 15−150°. The behavior of I_{VV} represents strong evidence of a decrease of the solvent quality as the temperature is decreased, which suggests that this system becomes more strongly interacting as the temperature is reduced. Further, the behavior of I_{VH} may indicate a strong increase of the orientational pair correlations, even at low concentrations. The intensity information points to the issue of association of the molecules; in such a case I_{VH} is very valuable, since it may suggest potential ways of how the molecules associate to form clusters. This issue will be discussed extensively in the subsequent sections.

Dynamic measurements at lower concentrations were also carried out in both toluene and chloroform (Figure 2, inset), from which the translational diffusion coefficient D_0 at infinite dilution, extrapolated at $q = 0$, was determined; the latter is assumed to be the self-diffusion. By using the relation of Broesma,[1,38] the contour length L of the rodlike PPP trimers can be determined, by assuming absolute stiffness and a certain value of the rod (trimer) diameter, d. This expression relates D_0 to the geometric characteristics of the trimers:

$$D_0 = \frac{k_B T}{3\pi\eta L}\left[\ln\left(\frac{2L}{d}\right) - \gamma\right] \qquad (7)$$

where γ is a function of the aspect ratio L/d. For the toluene solution, the measured diffusion coefficient is $D_0 = (3.41 \pm 0.22) \times 10^{-7}$ cm^2/s, while for the chloroform one, $D_0 = (5.65 \pm 0.44) \times 10^{-7}$ cm^2/s. Assuming $d = 17$ Å,[2,9] the corresponding values of L are 878 and 441 Å, respectively. It is noted that for polydisperse samples the *z*-average diffusion coefficient is actually measured, which for eq 7 is related to L_w. Further, from the value of L in toluene, which appears large, the rotational diffusion constant[1]

$$D_{r,0} = \frac{3k_BT}{\pi\eta L^3}\left[\ln\left(\frac{2L}{d}\right) - \zeta\right] \qquad (8)$$

where ζ is a function of L/d, can be calculated; its value is $D_{r,0} = 33\,757$ s^{-1} for $T = 25$ °C. The relevant characteristic time, $\tau_r = (6D_r)^{-1}$, is then estimated to be 5×10^{-6} s, indicating that the VH process should be observable inside the time window of the correlator. The fact that we do not get any VH dynamics strongly suggests that the aspect ratio of the scattering moieties is smaller; the diameter should be larger, and this represents more evidence of aggregation. The assumption of absolute stiffness can be relaxed by considering semistiff chains. In such a case, the Hearst−Stockmayer relations[1] are used:

$$D_0 = \frac{k_BT}{3\pi\eta_0 L}\left[\ln\left(\frac{L}{h}\right) + 0.166\left(\frac{L}{2l}\right) + \frac{h}{d} - 1\right] \qquad (9)$$

and

$$D_{r,0} = \frac{k_BT}{\pi\eta_0 L^3}\left[3\ln\left(\frac{L}{h}\right) - 7 + 4\left(\frac{h}{d}\right) + \frac{L}{2l}\left(2.25\ln\left(\frac{L}{h}\right) - 6.66 + 2\left(\frac{L}{h}\right)\right)\right] \qquad (10)$$

where h is the length of the repeating unit (14.9 Å), l is taken typically as 220 Å^3, and $d = 17$ Å. Application of eq 9 in the case of the solution in toluene leads to $L = 1050$ Å. Then, from eq 10 $D_{r,0} = 41\,837$ s^{-1} and $\tau_r = 4 \times 10^{-6}$ s, which is in agreement with the stiff-rod results above. Therefore, it can be concluded that chain flexibility (or rigidity) should not be the reason for the observed effects or the lack of VH dynamics in the time window available. Furthermore, from the measured diffusion constant in toluene and for an average $L_w = 650$ Å (as determined from static light scattering, using the wormlike model) we get a hydrodynamic diameter of $d = 60$ Å. Compared to the value of $d = 17$ Å considered above, this result is in agreement with the static results above, suggesting that the scattering moieties (in toluene) are rather small aggregates (typically trimers, as discussed before) lying parallel to each other. The actual number of molecules forming these small aggregates depends on the conformation of the molecules, and mainly the side chains, but on the basis of the above numbers, as well as the wormlike conformation of the macromolecules, the static and dynamic information on aggregation is consistent; but again, typically, they are trimers. This parallel alignment is not surprising, since this orientation is necessary for the van der Waals forces to dominate and aggregation to take place,[4,39] and is also consistent with the VH intensity behavior (Figure 2).

In concluding this section it can be stated that we have the means to determine the nature of dynamic processes taking place in dilute solution. However, for the system PPP/toluene even at concentrations as low as 0.084% by weight ($c/c^* \approx 0.76$), it is not possible to obtain single molecules; instead, small clusters are present, termed as trimers. Further, it is clear that interactions are of significant importance in this system, especially as the temperature decreases. This points to the need to study systematically the formation of associations at higher concentrations.

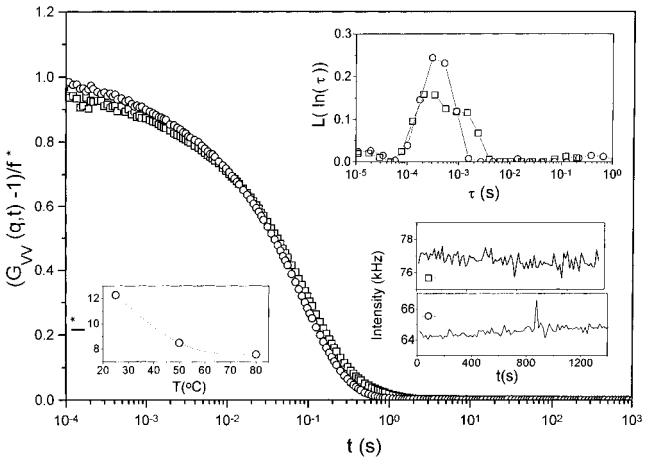

Figure 3. Polarized (VV) intensity correlation functions for a 3.9% by weight PPP solution in toluene, at a scattering angle of 45° and a temperature of 25 °C, before (squares) and after (circles) a temperature treatment at 80 °C. Corresponding distribution of relaxation times and intensity profiles during the experiments are depicted in the upper and lower right insets, respectively. The mean total polarized intensity normalized to that of toluene, I^*, is shown at different temperatures in the lower left inset.

B. Semidilute Regime. (i) Phenomenology. We now turn to the higher concentrations with the aim of investigating the dynamics of self-assembly of the hairy rods. We start with a semidilute solution of concentration 3.9% ($c/c^* \approx 35$), which was measured 6 days after preparation at three successive temperatures, namely 25, 50, and 80 °C, respectively. It is noted that, before each measurement, the samples were always left to equilibrate, as already mentioned. Results in terms of $G_{VV}(q,t)$ and the distributions $L(\ln \tau)$ (eq 3) are depicted in Figure 3. It is noted that all $G_{VV}(q,t)$ shown in this paper have been corrected for the instrumental factor f^* and hence represent net normalized intensity time correlation functions. At the end of the measurements, the sample was left at 80 °C overnight and measured again the second day after cooling at the same temperature.

It is clear that on the first day there is a second process at 25 °C, slower than the main one; the latter is attributed to cooperative diffusion of the rigid rods. This extra process seems to be an induced one, since it disappears with increasing temperature. Further, it does not reappear on the second day, upon cooling to 25 °C and keeping the solution at that temperature for 24 h. The corresponding total intensity for the second day increases (by about 60%) as the temperature drops from 80 to 25 °C and is depicted in the lower left inset of Figure 3. Further, in the temperature range studied (25−80 °C) the dynamics of the main process scales with the solvent viscosity. This suggests that, besides the disappearance of the extra slow process, no breakup of the original scattering moieties, i.e. trimers (in the "entangled" state), takes place at the specific concentration, as the temperature increases.

The presence of the extra slow process originally at 25 °C, together with its disappearance at 80 °C and the corresponding intensity behavior, represents evidence

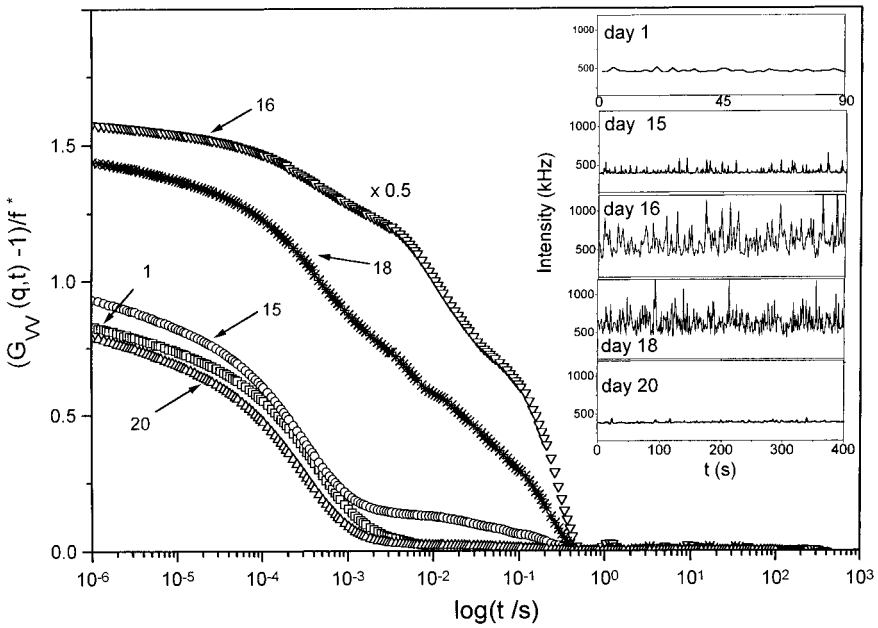

Figure 4. Polarized intensity correlation functions for a 4% by weight PPP solution in toluene, at a scattering angle of 45° and a temperature of 10 °C, at various elapsed times from solution preparation, namely the 1st, 15th, 16th, 18th, and 20th days (indicated by the arrows). The correlation function of the 16th day exhibits a pronounced contrast and is divided by 2 (×0.5) for clarity. Inset: Traces of the corresponding total scattering intensities.

of the significance of the role of the thermodynamic interactions in this phenomenon, which appears to be time-dependent. Further, it is noted that the temperature treatment described in Figure 3 leads to a $G_{VV}(q,t)$ at 25 °C with no extra process within at least 24 h, indicating a way to obtain a semidilute solution without additional intermolecular processes (among trimers, as discussed in the dilute regime section) within a certain time; this is important for studying molecular (rather trimer) dynamics under such conditions. The above information suggests that interactions in the system are increased at lower temperatures (while dynamics still probes only one molecular—rather trimer—relaxation process), and this of course brings up the issue of phase separation, which will be discussed in subsequent sections.

(ii) Kinetics of Aggregate Formation. Using the information from Figures 2 and 3, it was decided to perform these investigations at 10 °C and a concentration of 5% ($c/c^* \approx 45$), since under these conditions the observed effects are anticipated to be more dramatic. The solution was left for at least 1 day at 80 °C to break up any potential intermolecular aggregates, as confirmed by the single relaxation process at that temperature. It was then cooled down to 10 °C, where successive static and dynamic light scattering measurements were carried out for a period of about 3 weeks. Figure 4 shows the time evolution of the $G_{VV}(q,t)$ for this solution at a scattering angle of 45°. The first day corresponds to the fresh solution, pretreated at 80 °C, as already described, and measured within 24 h after reaching the final temperature of 10 °C. Only one relaxation process appears, which is attributed to the cooperative diffusion of the molecules (trimers) in the semidilute solution. This process has a characteristic time which remains constant at about 0.5 ms, from the first to the 15th day. However, with elapsed time we observe an additional slow process (third day), which appears to be more pronounced as time evolves and comprises actually two separate relaxation modes (15th day). Meanwhile, the total intensity (inset of Figure 4) increases and exhibits significantly larger fluctuations. On the 15th day, the second process, which we call "slow", has a characteristic time in the range of 20 ms, while the third one, which we call "ultraslow", has a characteristic time of about 350 ms.

From this discussion, it follows that the time of the evolution of these processes is of the order of 2 weeks. The $G_{VV}(q,t)$ of the 15th day indicates that the first process is a stretched exponential (eq 4), with a typical value of the shape parameter $\beta = 0.7$. This is expected, since in semidilute solution the coupling between rotation and translation or other relaxation mechanisms, may interfere with the cooperative diffusion, in addition to polydispersity effects.[2] The slower processes can be characterized either from the $G_{VV}(q,t)$ of the 15th day or from the corresponding one right after the disturbance (e.g. 16th day), as discussed below. The second slow process is typically nearly single exponential or slightly steeper ($\beta = 1.1$), while the main characteristic of the third ultraslow mode is its clearly steeper than single exponential shape; when fitted with a KWW function (eq 4) it gives a shape parameter with a typical value of $\beta = 1.4$. Further, the times of the three processes, exhibit different q dependencies, as discussed in section C below.

The formation of clusters, related to the slow and ultraslow processes, was accompanied by sedimentation. This was observed visually, by gently removing the sample cell from the light scattering setup, at the end of the 15th day. A cloudy off-white sediment was apparent in the bottom of the sample cell, filling a small volume fraction of the solution. When the sample was examined by PCS after 1 h, the amplitude of the two slow processes, as well as the total intensity and its fluctuation increased substantially, as can be seen in Figures 4 and 5 and their insets. Meanwhile, the amplitude of the main process is apparently decreased. Note that in Figure 4 one correlation function (16th day) is divided by 2, since its contrast is very high, as discussed below (section C). This dramatic effect is certainly due to the slight disturbance of the sample, associated with the gentle removal of the sample cell from the goniometer setup and its subsequent return. As a result of that, some clusters, probably mostly from the top surface of the sediment, break apart from it and

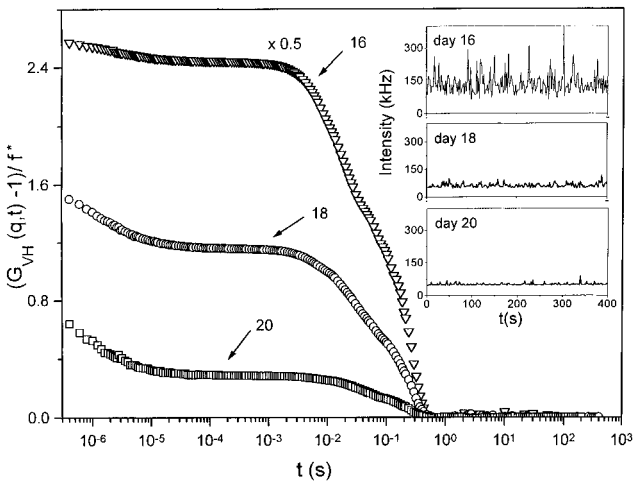

Figure 5. Depolarized intensity correlation functions for the 4% by weight PPP solution in toluene, at 45° and 10 °C, at the 16th, 18th, and 20th days (indicated by the arrows), from solution preparation. The correlation function of the 16th day exhibits a pronounced contrast and is divided by 2 (×0.5) for clarity. Inset: Traces of the corresponding total scattering intensities.

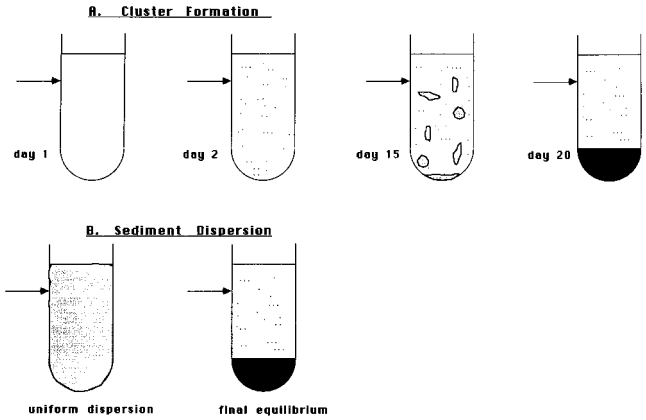

Figure 6. Schematic of the measured PPP sample, illustrating the position of measurement and formation and sedimentation of the cloud (A) or the dispersion of the sediment and settling of a uniform suspension (B). Arrows indicate the position of PCS measurement. (A) Cluster formation: (day 1) homogeneous solution; (day 2) aggregation nuclei formed; (day 15) cloud formation; (day 20) final equilibrium between sediment and top clear solution. (B) Sediment dispersion: (uniform dispersion) immediately following shaking; (final equilibrium) sediment with top clear solution, after about 1−2 h, depending on shaking.

are redispersed to the top solution giving rise to additional intensity fluctuations, as well as enhanced average intensity and contrast. Eventually, at steady state these dispersed clusters will settle down, as will be discussed below, in (iii).

An additional feature associated with the extreme sensitivity of the correlation functions to mechanical disturbance, is the fact that the increased contrast of the slow modes now provides a means to characterize them systematically; this was a rather difficult task to do before this disturbance, as can be inferred from the correlation function of the 15th day (Figure 4). From Figures 4 and 5, it is apparent that during the 16th day the slow and ultraslow processes are very pronounced, but they decrease with time rather significantly; for instance, on the 18th day, their contrast has dropped. Finally, on the 20th day, i.e. 5 days after the sample disturbance, the fast main process dominates the correlation function, whereas the total intensity is decreased and becomes smooth (no fluctuations). This behavior is clearly a result of the sedimentation of aggregates and any potential larger formations, which appear as the off-white cloud, dispersed in the solution. The q dependence of the dynamics of the various processes is unaffected: the fast process is q^2-dependent, the slow weakly q-dependent, and the ultraslow one almost q-independent. It should be mentioned, however, that it is difficult to determine the characteristic times with high accuracy, due to the uncertainty involved in the experimental procedure.

In this context it must be noted that although it is widely recognized that the optimum way to analyze the experimental $G(q,t)$ is by means of the ILT analysis (eq 3), the treatment of the $G(q,t)$ exhibiting cluster modes was carried out using a double or triple KWW fit (eq 4), and not ILT, since the correlation functions of the slow processes are sharper than single exponential. The characterization of the slow and ultraslow modes is completed by measuring the dynamics in the VH geometry, as seen in Figure 5. The tail seen in Figure 5, just at the fast edge of the time window of the correlator, is real and represents the fast VH process due to molecular reorientation, which slows down significantly with increasing concentration of the rodlike chains.[1,2] Setting this mode aside, we clearly see two slow VH processes, with intriguing similarities with the respective VV relaxation functions: they lose amplitude from the 16th to the 20th day; their times are the same in magnitude as the corresponding VV times, within experimental error. The fact that both slow and ultraslow processes are VH active indicates that they are anisotropic; this suggests possible ways of formation of the clusters and larger associations. As already mentioned, when the slow and ultraslow processes were dominant in the period between the 16th and 18th days, both in VV and VH (Figures 4 and 5), the total contrast exceeded the full contrast of our setup. The only explanation that can be given at this point is the statistical bias due to the presence of large and sudden fluctuations of the scattered intensity; this breaks up the translational time invariance of the scattered intensity, and as a result the process is no longer "stationary stochastic".[40] Under these circumstances, the Siegert relation (eq 1) may not hold anymore. This problem makes the calculation of the amplitudes of the relaxation processes somehow ambiguous. To overcome this difficulty, we assume that the contrast of the fast well-resolved (in the polarized geometry) process is true and that the rest of the contrast needed to reach full contrast is split into the two extra processes according to their apparent contrasts. Results of the amplitude analysis are discussed in section C.

Before proceeding with the detailed discussion of the nature of the aggregation modes and the heating cycle and sedimentation studies, it is illustrative to explain the physical layout of these investigations. As can be seen schematically in Figure 6A, the static and dynamic experiments on cluster formation "look" at a fixed position of the sample cell, near the top surface (indicated by the horizontal arrow). At the beginning of the kinetic experiment, the sample is homogeneous, as in day 1, for instance (see also Figure 4). Then, with time some aggregation nuclei are formed, which may cross the probe volume, on day 3 for example. Later, on day 15, some clouds are formed, which seem to be in equilibrium with smaller moieties. Finally, sedimentation of the various associations (also clouds) takes place; there is a large concentration gradient toward the bottom of the sample, and eventually at steady state

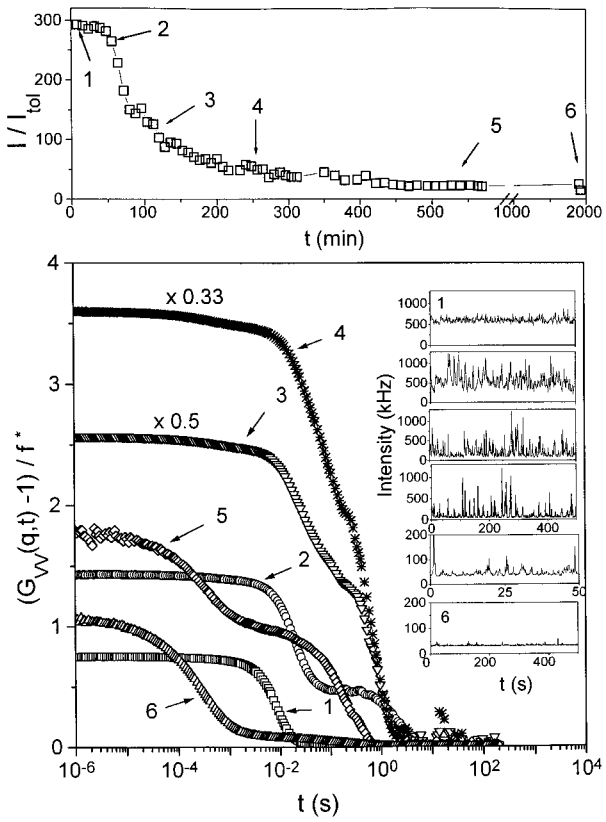

Figure 7. Upper part (a): Polarized light scattering intensity, normalized by the polarized intensity of toluene, as a function of time, after a macroscopically uniform suspension was obtained through sediment dispersion (Figure 6B). The arrows indicate the times at which polarized intensity correlation functions were recorded: (1) 10 min; (2) 45 min; (3) 2 h; (4) 4 h; (5) 9 h; (6) 32 h. The sediment resulted from aggregation of PPP in a 5% toluene solution. Measurements were carried out at a scattering angle of 45° and a temperature of 25 °C. Lower part (b): Relevant correlation functions along with their corresponding traces of the total scattering intensity. All measurements were carried out under steady state. The correlation function of the 2nd and 4th hours exhibit a pronounced contrast and are divided by 2 (×0.5) and 3 (×0.33) for clarity. Arrows indicating times correspond to those of the upper part (a).

there is a top clear solution in equilibrium with the sediment, at day 20.

(iii) Intervention of Sedimentation. It is now clear that since the associations settle under gravity once they grow beyond a certain size, understanding the sedimentation process is a crucial task. To this end, the behavior of the semidilute phase-separated system (with the sediment, at the end of the 20th day) was studied systematically at various temperatures, in order to determine the "onset-of-melting" temperature, corresponding to a single relaxation process, as discussed below. The first temperature examined was 25 °C. The situation is illustrated schematically in Figure 6B, where the two-phase system was agitated manually in order to obtain a macroscopically uniform suspension. Due to the extreme sensitivity of the system under investigation to mechanical disturbance, it is obvious that these shaking experiments are not quantitatively reproducible. This means that the characteristic times for the beginning and end of the transient settling regime are not reproducible, but vary depending on the shaking. Nevertheless, the physical picture remains unchanged. A typical sedimentation kinetics experiment is illustrated in Figure 7a, which depicts the total scattered VV intensity, normalized to the polarized intensity of toluene at 45°, as a function of time. Initially, the sample is uniformly dispersed and the intensity is constant. After about 1 h settling has started and becomes evident through the sharp decrease of intensity. Eventually, after about 200 min the intensity reaches a lower plateau, indicative of steady state. From this experiment, we can determine when steady (upper and lower plateau) or transient conditions have been reached. Further, the upper plateau corresponds to multiple scattering, as will be discussed in the next section, since the sample is opaque, due to the dispersed clusters which form a macroscopically uniform dispersion. The lower plateau corresponds to a homogeneous solution, more dilute than the original 5% one, in equilibrium with the sediment, where practically one main relaxation process is observed. Finally, in the transitional regime the settling of the aggregates gives rise to large intensity fluctuations. These aspects are addressed in the following sections.

The real time behavior of the dispersed sediment in terms of sedimentation is described in Figure 7a, discussed above. Characteristic results from PCS measurements of VV dynamics are depicted in Figure 7b. The first intensity correlation function, taken from the uniform dispersion corresponds to the upper intensity plateau, at about 50 min (referring to Figure 7a). The nearly opaque dispersion gives rise to multiple scattering, as confirmed by the low transmitted intensity (about 8%), the identical VV and VH correlograms, and visual observation. The relevant intensity trace was rather smooth and stable. The correlation function exhibits one dominant relaxation process, which is clearly sharper than single exponential (β varies between 1.6 and 1.9), and a rather weak slow process (Figure 7b). For the first hour, the intensity decreases only slightly with time (nearly constant), but there is a significant increase of fluctuations (insets of Figure 7b). After 55 min this increase becomes dramatic and the correlation function exhibits clearly a slow process with significant amplitude, while the process seen under multiple scattering conditions is slowed down with respect to the first measurement. After the first hour the intensity starts decreasing sharply, and at the end of the third hour it drops to $^1/_6$th of its initial value.

The polarized intensity correlation functions after 2 and 4 h (Figure 7b) consist of three processes: the fast cooperative diffusion of the trimers, which can be barely observed due to its relatively low contrast, and the slow and ultraslow processes, both with very large contrasts. The second slow process has a shape parameter of $\beta \approx 1.1$, whereas the third ultraslow one is even steeper, with $\beta \approx 1.4$. The corresponding intensity has dropped, due to sedimentation, and the intensity fluctuations are high. These fluctuations can be seen by eye as large spikes in the scattering volume (and may be due to the large moieties which are translating or reorienting in and out of the illuminated volume). After 9 h the intensity has dropped substantially, and the large fluctuations are more rare. The two slow processes lose amplitude and are not easily discriminated anymore, whereas the fast diffusive process becomes now dominant. After 32 h, the intensity is almost constant and the correlation function reveals the main fast process ($\beta \approx 0.7$) and an extra very small slow relaxation, which comprises the slow and ultraslow processes.

(iv) Heating and Cluster Breakup. We have repeated the above experiment (statics and dynamics) at various temperatures above 25 °C, in order to determine the temperature corresponding to the melting of the associations. At 40 and 50 °C the solution was observed for a few days. The decrease of the intensity

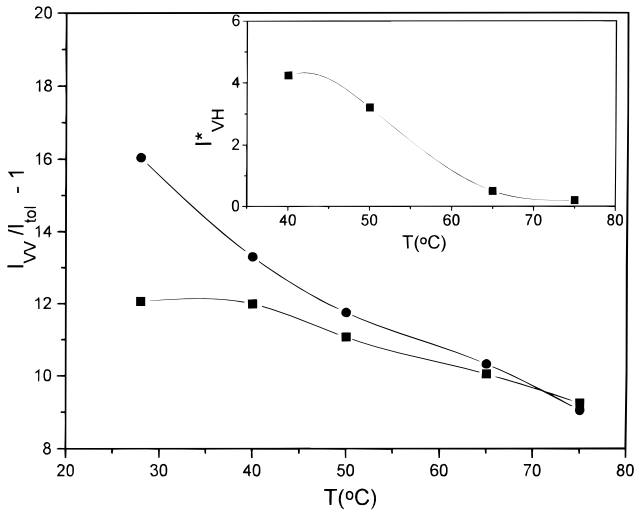

Figure 8. Total polarized scattering intensity from a 5% PPP solution in toluene, normalized to the corresponding intensity of toluene, as a function of temperature and time. Circles (●) and squares (■) refer to the first and last (5th or 6th) days of measurement at each temperature. Inset: Total depolarized scattering intensity (I^*_{VH}) from the 5% PPP solution in toluene, normalized to the corresponding intensity of toluene, as a function of temperature, at the last day. Solid lines are drawn to guide the eye.

occurred just after the first day (corresponding to the uniform dispersion of Figure 6B), and the correlation functions revealed the same dynamics as in the case of 25 °C, suggesting that on the average the clusters did not break up. At 65 °C the solution became clear immediately, but a further decrease of the intensity, accompanied by a decrease of the amplitude of the slow process was observed. The corresponding VH correlation function also exhibits a decrease of the amplitude of the slow processes. No sediment was apparent visually at the bottom of the sample cell. This can be explained by both a melting of most of the last aggregates and/or their sedimentation (which is minimal, and thus does not produce any visually observed sediment). Finally, the solution was agitated and put at 75 °C. There was a slow process (small in amplitude) apparent in the VV and the VH function which disappeared after 3 days. It is important once again to note the sensitivity of the VH dynamics to these experiments. This heating−dissolution experiment is better illustrated in Figure 8, which depicts the total polarized intensity of the scattering moieties, normalized by that of toluene, as a function of temperature and time. Actually, by time we refer to the first and last measurements; the latter were undertaken between the 3rd and 6th day, depending on the temperature. It can be clearly observed that above 65 °C steady state was reached immediately, suggesting that this temperature corresponds to dissolution (complete breakup of the aggregates). Further, from the intensity ratio of the first and last measurements, we can obtain the change of concentration of the upper phase (referring to Figure 6A) with temperature. As the temperature rises from 28 to 75 °C, the concentration increases from 3.8% to 5% by weight. The inset of Figure 8 depicts the total steady state (in final equilibrium) VH intensity as a function of temperature. This plot represents an unambiguous way to determine the melting temperature, where all aggregates are broken apart, and we are back to the homogeneous solution of trimers.

C. Aggregation Modes. In order to characterize the slow and ultraslow relaxation modes, their q dependence was investigated at the three extreme cases: (a) at $t = 0$, corresponding to the cloudy dispersion, where multiple scattering dominates; (b) at $t = 3$ h, corresponding to the transient settling regime, where the contrast is pronounced; and (c) at $t = 30$ h, corresponding to the lower intensity plateau, where the usual single scattering conditions are established. It is noted that the measurements in the transient regime were carried out at a different time than those of Figure 7, and hence the corresponding relaxation rates of the slow and ultraslow modes are different. Nevertheless, the underlying physics behind these processes is the same, as already discussed and will be seen below.

(i) Initial Regime: Multiple Scattering. In this regime, the dynamics is practically q-independent, and nearly the same, in both the VV and the VH geometry. The sample is opaque and the transmission, $T = I/I_{tol}$, measured with a power meter (with a sensitive area of radius 1 cm, in a distance of about 12 cm from the sample cell) in the forward direction is about 8% in case a and about 60% in case c. It is thus apparent that light is scattered multiply from our sample, and that the single scattering formalism cannot be applied here. On the other hand, the sample, although opaque, is not milky, allowing thus the path of light to be observed; this suggests that in this situation we have not yet reached the limit of light diffusion in the sample, which can be treated quantitatively using the theory of diffusive wave spectroscopy (DWS).[41] Furthermore, although the transmission from a multiply scattered sample in a slab geometry is $T = (5l^*/3L)/(1 + 4l^*/3L)$ (where l^* is the transport mean free path, i.e. the length scale at which the direction of light is randomized,[41] and L is the thickness of the slab), yielding $l^* = 0.05\ L$, which is a reasonable number for applying DWS, this is not the case in the present experiment. The reason has to do with the geometry of the scattering cell used (cylindrical), as well as the way the actual transmission measurement was carried out, which did not measure the light transmitted and scattered by the last scatterer in a solid angle of 2π in the forward direction, but rather only a part of it. Given the above complications, in lack of another alternative, we try to assess the experimental observations qualitatively, and start from the theory of DWS, according to which the light is assumed to follow a random walk inside the scattering medium, and the scattered field autocorrelation function is given by:[41]

$$C(t) = \left\langle \sum_p \frac{|E_p|^2}{\langle I \rangle} \exp(-i\Delta\phi_p(t)) \right\rangle \qquad (11)$$

where E_p is the amplitude of the scattered electric field along a path with p scattering events, $\langle I \rangle$ the average total scattered intensity at the detector, and $\Delta\phi_p(t)$ is the phase shift of light along the path p.

In the case of independent successive scattering events, caused by scatterers undergoing Brownian motion, and independence of the scattering wavevector q_i from the displacement of the scatterer $\Delta r_i(t)$, we get

$$C(t) = \int P(s) \exp\left(-\frac{1}{3}k_0{}^2\langle \Delta r^2(t)\rangle \frac{s}{l^*}\right) ds \qquad (12)$$

where s is the length of the path of the light, $P(s)$ is the probability that light will follow this path, k_0 is the scattering wavevector at an angle $\theta = 180°$, and $\langle \Delta r^2(t)\rangle$ is the mean square displacement of the scattering particle, which in the diffusion limit here is given by $6Dt$ with D being the diffusion coefficient.

In the case of a scatterer in a velocity field (here, due to sedimentation) we have[41]

$$\Delta\phi_p(t) = kt\sum_{v=1}^{p}\hat{e}_v[\bar{V}(\bar{R}_v) - \bar{V}(\bar{R}_{v+1})] \qquad (13)$$

where $\hat{e}_v$ stands for the unit vector corresponding to the light beam which emerges after the vth scattering event, and $\bar{V}$ is the velocity of a scatterer at position R_v. It is thus evident from eq 12 that only a velocity gradient, Γ, within the probe volume can produce a phase change; in other words, in this case we detect the velocity gradient of moving particles. The corresponding correlation function is then

$$C(t) = \int P(s)\exp\left(-\frac{sl^*}{30}k_0^2\Gamma^2t^2\right)ds \qquad (14)$$

Comparing eqs 12 and 14, it is important to note the t^2 dependence in the case of velocity gradient detection, which in a sense relates to a deterministic motion, as opposed to the t dependence in the case of random Brownian motion. Further, we emphasize again that the quantity related to the phase shift in the former case is the velocity gradient and not the diffusion coefficient (which is associated to the Brownian motion).

From eq 14 it is apparent that the decay of the correlation function is faster, the larger the path s is. This happens because in multiple scattering each particle in the light path has to move only a small distance in order for the entire path length to change by one wavelength. Thus longer light paths give shorter decay times. Further, the decay rate depends on the scattering geometry (at different scattering angles the light paths are different), rather than the scattering wavevector directly. Thus, DWS predicts a decrease of the characteristic time of a relaxation process under multiple scattering conditions, compared to the same process in the single scattering limit. This behavior conforms with our experiments, as judged from the correlation functions of Figure 7b. As the sedimention proceeds with time, and the single scattering conditions are approached, the relaxation process of the multiple scattering case (a) becomes significantly slower. In addition, the shape of the correlation function becomes less steep, approaching a single exponential decay (Figure 9a); this can be explained by the fact that during the initial stage (a) we observe the motion of clusters in a flow field (sedimentation), whereas in the late stage (c) we mainly observe clusters undergoing Brownian motion in the clear phase (single scattering; sedimentation is absent). The experimental data at various angles between 15 and 150° reveal a nearly q-independent dynamics; the characteristic relaxation rate at $q = 0$ is found to be about 500 s^{-1}. From the fitting of the correlation function we obtain the shape parameter $\beta = 1.9$, which practically suggests that we are in the velocity gradient limit (deterministic motion).

(ii) Intermediate Regime: Single Scattering Limit. The main findings are depicted in Figure 9b. Referring to the dynamics, depicted in Figure 9a,b, the slow mode exhibits a very weak q dependence in the relaxation rates, in both the VV and VH scattering, whereas the ultraslow mode is characterized by q-independent relaxation rates, in both the VV and VH geometries. In terms of the static picture, and referring to Figure 9b, the intensity of both the slow and the ultraslow process is strongly q-dependent, in both the VV and the VH, especially at low q's. Moreover, it is

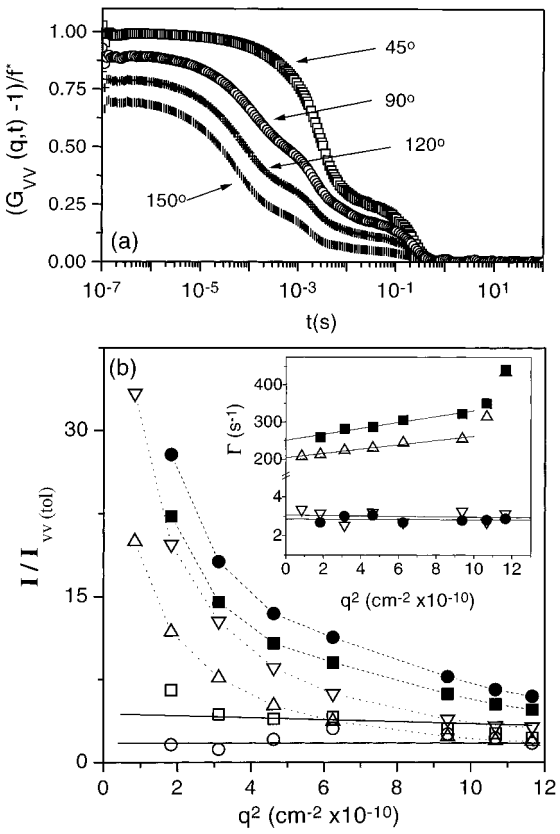

Figure 9. (a) VV intensity correlation functions in the intermediate single scattering regime (corresponding to transient settling in Figure 7a), at various scattering angles θ: 45° (□); 75° (○); 120° (+); 150° (|). (b) Polarized and depolarized intensities, normalized by the VV intensity of toluene, for both slow modes in the transient settling regime, following sediment dispersion, as functions of q^2. Key: VV slow (■); VV ultraslow (●); VH slow (△); VH ultraslow (▽); Isotropic contributions to VV intensity, I_{iso}: slow (□) and ultraslow (○). Inset: Corresponding relaxation rates Γ for the slow and ultraslow, measured in the polarized and depolarized geometries as a function of the scattering wavevector, q. Lines are drawn to guide the eye.

apparent that nearly all polarized light scattering intensity is due to the anisotropy of the scattering moieties. The former arises from both concentration fluctuations, which are isotropic (I_{iso}) and orientation fluctuations which are anisotropic (I_{VH}). For independently moving particles in an orientationally isotropic enviroment, in the absence of translation-to-rotation coupling and in the single scattering limit, the usual expression for the polarized scattered intensity is[34]

$$I_{VV}(q) = I_{iso}(q) + {}^4/_3 I_{VH}(q) \qquad (15)$$

For large scatterers, where intramolecular interference is important, the above relation does not hold always. Instead, there is an additional term, I_{coupl}, originating from a coupling of concentration and orientation fluctuations:[34]

$$I_{coupl} \approx N\alpha\beta_i\langle\sum_{i,j}^{n}(3\cos^2\theta_i - 1)\exp[iq(r_i - r_j)]\rangle \qquad (16)$$

where N is the number of scatterers, α is the polarizability, β_i is the inherent optical anisotropy, n is the number of segments, and r_i and θ_i are the position and angle of segment i of the scattering moiety, respectively.

This term always vanishes at $q = 0$, or for scatterers with completely randomly orientated segments.

The isotropic contribution estimated by substracting only the $^4/_3$rds of the VH intensity (according to eq 15) is small for both the slow and ultaslow process (Figure 9b, inset); actually it amounts to about 15% of the VV intensity, except in the high q's where it can reach 30%. In our experiments the extra term I_{coupl} (eq 16) is probably also important, making thus the actual contribution of the isotropic intensity even smaller. This strongly suggests that the two aggregate processes originate essentially from the anisotropic part of the scattering intensity. Further, it is noted that the amplitude ratio of the two processes ($\alpha_{slow}/\alpha_{ultraslow}$, where α is the amplitude of a particular relaxation process) remains nearly constant. More specifically, in the VV geometry it is about 0.8, whereas in the VH geometry it is about 0.6, for all scattering angles between 30 and 150°. Moreover, this ratio does not change with time, within the same sedimentation regime (transient or plateau).

The combined information on intensities and rates provides the following picture of the light scattering mechanism of the aggregate processes (slow and ultraslow): Both have the same origin (due to the same amplitudes), which is the orientational fluctuations of the scattering moieties. The slow mode has a shape parameter only slightly above 1 (Figure 9a), and thus it can be attributed to rotational diffusion; it is treated as a single exponential relaxation. The VH field correlation function under the assumption of independent translational and rotational diffusion is given by[34]

$$C(q,t) \approx N\beta_i^2 \exp[-(6\Theta + Dq^2)t] \qquad (17)$$

where Θ and D are the rotational and translational diffusion coefficients, respectively. From the measured rates in Figure 9a, we get $\Theta = 34\ s^{-1}$ and $D = 5 \times 10^{-10}$ cm^2/s. A single size R_H cannot account for these values through the usual expressions (for stick boundary conditions[42]), namely $\Theta = k_BT/(^4/_3)\pi\eta R^3$ and $D = k_BT/6\pi\eta R_H$, respectively. Thus, in order to rationalize these findings, we consider the diffusion coefficients for ellipsoids.[34,42] In particular, for an oblate ellipsoid with large axis b and small axis a, the translational and rotational diffusion coefficients are given by

$$D = \frac{k_BT}{6\pi\eta a}G(\rho) \qquad \text{and}$$

$$\Theta = \frac{3k_BT}{16\pi\eta a^3}\left(\frac{(2-\rho)G(\rho)-1}{(1-\rho^2)}\right) \qquad (18)$$

with $G(\rho) = (\rho^2 - 1)^{1/2}\ \rho \arctan[(\rho^2 - 1)^{1/2}]$ and $\rho = b/a$. Using the above experimental values of Θ and D, we get $a = 5590$ Å and $b = 5785$ Å. This result suggests that scattering originates from slightly deformed spherical clusters with a hydrodynamic radius of about 5700 Å. For a moiety of such a size, qR_g in the light scattering range is between 2.7 and 19.6, and therefore the form factor, independent of the shape, is already vanishingly small (below 0.2).[34] Moreover, the experimental evidence apparently suggests that clusters are rather loose structures, compared to their high optical anisotropy; therefore, it is expected that the amount of solvent inside each cluster (among the constituent rods) is nonnegligible, making thus the refractive index contrast, dn/dc, very small. Thus, it is expected that the anisotropic contribution in the intensity dominates over the isotropic one.

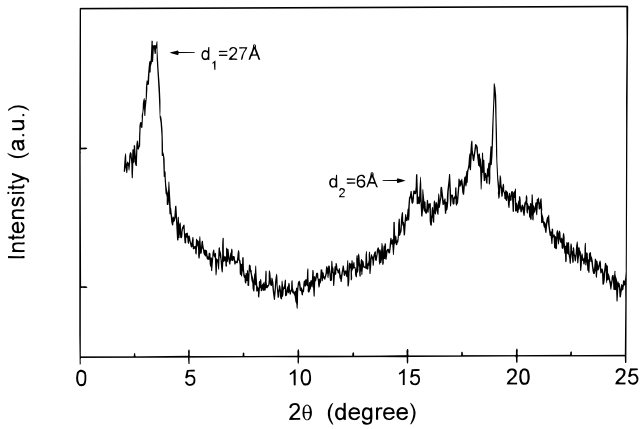

Figure 10. Scattered X-ray intensity from PPP sediment in toluene (produced from a 5% solution), as a function of scattering angle (2θ), indicating crystalline structure. Values of d_1 and d_2 represent characteristic distances between macromolecular backbones and side chains, respectively.

The ultraslow process is clearly steeper than single exponential; this situation actually corresponds to an intermediate regime between the diffusion limit and the free translation limit. In such a case, quantitative evaluation of the data is presently not possible. By taking into consideration the presence of sedimentation, as already discussed, we propose that this process is due to sedimentation-induced number fluctuations,[34,43] i.e. large associations entering and leaving the probe volume. These moieties can be networks of anisotropic clusters settling under gravity, rather than diffusing randomly. The passage of the scattering moiety through the probe volume is a translational motion, which should give in the VV a translational diffusion process, in addition to the number fluctuation one. We argue, however, that this may not be visible in the VV due to the very small structure factor. The small dn/dc also supports the argument of a negligible VV process. Further, the number fluctuations are related to non-Gaussian concentration fluctuations, associated with a small number of particles in the scattering volume (also responsible for the increased contrast). We believe that the latter is indeed the case in our experiments, because the ultraslow process was observed after the settling process was in progress (roughly in day 15, corresponding to the intermediate regime, and referring to Figure 6A), meaning that the concentration in the area of the measuring point was already reduced. Further, number fluctuations can be VH active as well, simply due to the anisotropy of the clusters. This picture is in agreement with the strong q dependence of the scattering intensity, which implies that clusters are large.

Finally, case c exhibits exactly the same dynamic characteristics as case b above.

(iii) Tentative Interpretation of the Aggregation Process. In order to obtain a better undertanding of the structure of the aggregates, we performed X-ray scattering studies of the sediment. Typical results are depicted in Figure 10. It is interesting to note that the peak observed at low scattering angles is clearly sharper than what is usually expected in the nematic phase, whereas in contrast to the expected amorphous halo at higher angles, an extra structure in that range is also observed. This is also in contrast to direct powder diffraction measurements with the original material, which showed the sharp peak at low angles and the amorphous halo at high angles. From these measurements it can be stated that the aggregates do not form a nematic but rather a crystalline phase, characterized

by two length scales: the distance between macromolecular backbones ($d_1 = 27$ Å) and the distance between side chains ($d_2 = 6$ Å). Thus the conformation of side chains in the solvent seems responsible for the formation of crystallites. These findings are in harmony with the strong anisotropy of the slow aggregation modes discussed before. Further, it is noted that the fact that the PPP powder does not exhibit any side chain crystallinity implies that during the slow nucleation process resulting from aggregation, the side chains have time to arrange in a crystalline phase, in contrast to the situation of (quick) solvent casting, from which the powder was obtained.

A remaining question emerging from the above discussion is whether the structures inferred by the relaxation processes conform to the standard thermodynamic picture of polymer solutions. To answer this question, let us for simplicity assume that the hairy-rod macromolecules (each of length L) "like" to form clusters; each cluster is of length L and has a square front surface of side $\sim N^{1/2}$, N being the number of rods in a cluster. If γ_s and γ_f denote the surface tension of the side (with dimension $LN^{1/2}$) and front of the cluster, respectively, we have $\gamma_f \geq \gamma_s$. Then, the free energy gain ΔF of the cluster, relative to a homogeneous state of isolated rods, can be written as

$$\Delta F = N(-\Delta G_{melt}(\phi) + 2\gamma_f\sigma^2) + 4L\sqrt{N}(\gamma_s\sigma^2) \quad (19)$$

where $-\Delta G_{melt}$ is the free energy gain per rod on aggregating and σ is the rod diameter. Equation 19 suggests that when $2\gamma_f\sigma^2 > \Delta G_{melt}$, there exists a metastable region where nuclei of any size are unfavorable, i.e. $\Delta F > 0$, independent of N. This result represents a clear departure from the conventional picture for flexible macromolecules, for which there is always a critical size N, beyond which $\Delta F < 0$ inside the two-phase region. The implication of this is that nucleation only happens for deep quenches. By considering now the situation where nucleation can occur, we can calculate the activation energy ΔF_{act} required to form a stable nucleus, from eq 19 by considering $\partial(\Delta F)/\partial N = 0$. In the case $\Delta G_{melt} \gg 2\gamma_f\sigma^2$, this leads to

$$\Delta F_{act} = \frac{(2L\gamma_s\sigma^2)^2}{\Delta G_{melt}} \quad (20)$$

By assuming $\Delta G_{melt} = L\Delta G^{seg}_{melt}$, where ΔG^{seg}_{melt} is the melting (or association) energy per segment, the above equation reduces to

$$\Delta F_{act} = L\frac{(2\gamma_s\sigma^2)^2}{\Delta G^{seg}_{melt}} \quad (21)$$

The above analysis indicates that the nucleation probability of rodlike polymers is lowered when compared to their flexible counterparts, and most importantly that the activation barrier for rodlike polymers is larger than for their flexible counterparts, since it increases with rod length. This in turn suggests a slow rate of nucleation, which is indeed observed experimentally. Furthermore, the above assumption of cluster length L can be reconsidered. It is now clear that nucleation cannot proceed with individual rods lined up end to end, since there is no free energy gain in such a process. On the other hand, two clusters (of length L) can come together end-to-end, since this will minimize the front surface energy. The question is whether it is possible to form clusters of one rod length or not. To resolve this, we have to decide whether a typical cluster is of size L or $L_c \gg L$. When two rods, each of length L, are coming together, they are approximately in parallel configuration, as already discussed.[4,39] The time for the rods to line up is L^2/D, where D is the diffusion coefficient. If this time is shorter than the average time between collisions, we have formation of clusters of size L, otherwise of size L_c. The latter time is approximately $c^{-2/3}/D$, where c is the average number concentration of rods per volume. Thus, for $L^2/D < c^{-2/3}/D$, or $c < 1/L^3 = c^*$, clusters of one rod length will be formed; this is of course not favorable due to the side surface free energy barrier (eq 20), as already discussed. However, for $c > c^*$, clusters of length L_c will be formed. This is the typical case of aggregation proceeding by nucleation-and-growth, which has been observed in our experiments. Thus, in the dilute regime, no aggregation takes place. As the concentration increases, in the semidilute regime, aggregation is possible with slow growth, leading to formation of large clusters with nearly parallel association, and/or networks of clusters associating end-to-end. This thermodynamic analysis, which captures the main features of the association dynamics, observed experimentally, is actually consistent with the formation of large aggregates (more than 30 associating molecules); it cannot account for the trimers formation.[44]

V. Concluding Remarks

The association dynamics of toluene solutions of a hairy-rod poly(*p*-phenylene) with flexible dodecyl side chains has been investigated thoroughly by photon correlation spectroscopy in the polarized (VV) and depolarized (VH) modes and by static light scattering. Toluene was found to be not a good solvent. In the dilute regime, molecules are assembled into small aggregates consisting of about three to four molecules in parallel configuration, termed trimers. In the semidilute regime, two new relaxation processes were found, which appeared at room temperature after about 1 week from the preparation of the solution, and disappeared with heating at about 65 °C. They are attributed to the formation of clusters, of typical size 570 nm. The substantial VH sensitivity indicates strong anisotropy of the aggregates, which are crystallized, as revealed by X-ray scattering. In both the VV and VH, the slow process is characterized by weakly q-dependent dynamics and strongly q-dependent intensity, and the ultraslow one exhibits q-independent dynamics and strongly q-dependent intensity, whereas the amplitude ratio of the two processes is essentially constant. These processes are steeper than single exponential decay with $\beta \approx 1.1$ and 1.4 for the slow and ultraslow, respectively. They are related to the orientational fluctuations of the clusters, giving rise to slow reorientational motion with negligible isotropic contribution, and ultraslow number fluctuations of the anisotropic aggregates. A simple thermodynamic analysis suggests that rodlike macromolecules exhibit a larger activation energy barrier compared to their flexible counterparts, in agreement with the experimental evidence. Furthermore, the first stages of sediment redispersion exhibit multiple scattering with a steeper than exponential relaxation process ($\beta \approx 1.9$), associated with a sedimentation-induced velocity gradient in a transient pseudonetwork formed by the dispersed clusters. Finally, it is noted that the association processes described here are reversible, since a heating cycle to 65 °C leads to cluster breakup and a single relaxation process of the trimers in semidilute solution.

Acknowledgment. Professor M. Ballauff (University of Karlsruhe) is thanked for kindly providing the polymers used in this work. This research was partially supported by the EC, BRITE/EURAM program (contract BREU CT91-0505), and the Greek General Secretariat for Research and Technology (GSRT: Basic Research). We are grateful to Professor G. Maret (University of Konstanz) and Dr. A. Skoulios (IPCMS, Strasbourg) for stimulating discussions and to Dr. R. Seghrouchni and Dr. B. Loppinet for their assistance with the X-ray measurements. S.K. was visiting FORTH during the summer of 1995, when some of this research was performed, and he appreciates their warm hospitality.

References and Notes

(1) Doi, M.; Edwards, S. F. *The Theory of Polymer Dynamics*; Oxford Science Publishers: Oxford, 1986. Tracy, M. A.; Pecora, R. *Annu. Rev. Phys. Chem.* **1992**, *43*, 525. Russo, S. P. In *Dynamic Light Scattering*; Brown, W., Ed.; Oxford Science Publications: Oxford, U.K., 1993.
(2) Petekidis, G.; Fytas, G.; Witteler, H. *Colloid Polym. Sci.* **1994**, *272*, 1457.
(3) Tiesler, U.; Rehahn, M.; Ballauff, M.; Petekidis, G.; Vlassopoulos, D.; Maret, G.; Kramer, H. *Macromolecules* **1996**, *29*, 6832. Petekidis, G.; Vlassopoulos, D.; Galda, P.; Rehahn, M.; Ballauff, M. *Macromolecules* **1996**, *29*, 8948.
(4) van der Schoot, P.; Odijk, T. J. *J. Chem. Phys.* **1992**, *97*, 515.
(5) Wegner, G. *Mol. Cryst. Liq. Cryst.* **1993**, *235*, 1. Ballauff, M. In *Materials Science and Technology*; Cahn, R. W., Haasen, P., Kramer, E. J. Eds.; VCH: Weinheim, 1993. Ballauff, M. *Angew. Chem.* **1989**, *28*, 253.
(6) Jamieson, A. M.; Southwick, J. G.; Blackwell, J. *Faraday Symp. Chem. Soc.* **1983**, *18*, 131.
(7) Ferrari, M. E.; Bloomfield, V. *Macromolecules* **1992**, *25*, 5266.
(8) Weissenburg, P.; Odijk, T.; Cirkel, P.; Mandel, M. *Macromolecules* **1995**, *28*, 2315. Weissenburg, P.; Odijk, T.; Cirkel; P.; Mandel, M. *Macromolecules* **1994**, *27*, 306.
(9) Richtering, W.; Gleim, W.; Burchard, W. *Macromolecules* **1992**, *25*, 3795.
(10) Meyer, E. L.; Fuller, G. G.; Clark, R. C.; Kulicke, W.-M. *Macromolecules* **1993**, *26*, 504.
(11) Wegner, G.; Mathauer, K. *Mater. Res. Soc. Symp. Proc.* **1992**, *247*, 767. Embs, F.; Funhoff, D.; Laschewsky, A.; Licht, U.; Ohst, H.; Prass, W.; Ringsdorf, H.; Wegner, G.; Wehrmann, R. *Adv. Mater.* **1991**, *3*, 25. Miller, J. S. *Adv. Mater.* **1990**, *2*, 601. Wu, J.; Lieser, G.; Wegner, G. Submitted for publication.
(12) Russel, W. B.; Saville, D. A.; Schowalter, W. R. *Colloidal Dispersions*; Cambridge University Press: Cambridge, U.K., 1989.
(13) D'Hene, P.; Mewis, J.; Fuller, G. G. *J. Colloid Interface Sci.* **1993**, *156*, 350.
(14) Weitz, D. A.; Oliveria, M. *Phys. Rev. Lett.* **1984**, *52*, 1433.
(15) Martin, J. E. *Phys. Rev. A* **1987**, *36*, 3415.
(16) Zhou, Z.; Chu, B. *J. Colloid Interface Sci.* **1991**, *143*, 356. Broide, M. L.; Cohen, R. J. *Phys. Rev. Lett.* **1990**, *64*, 2026.
(17) Carpineti, M.; Giglio, M. *Phys. Rev. Lett.* **1992**, *68*, 3327. Carpineti, M.; Giglio, M. *J. Phys.: Condens. Matter* **1994**, *6*, A329. Roux, P. W.; Woutersen, A. T. J. M.; Ackerson, B. J.; Kruif, C. G. D. *Physica A* **1989**, *156*, 876. Lin, M. Y.; Lindsay, H. M.; Weitz, D. A.; Ball, R. C.; Klein, R.; Meakin, P. *Phys. Rev. A.* **1990**, *41*, 2005.
(18) Allain, C.; Cloitre, M.; Wafra, M. *Phys. Rev. Lett.* **1995**, *74*, 1478.
(19) Warren, P. B.; Ball, R. C.; Boelle, A. *Europhys. Lett.* **1995**, *29*, 339.
(20) Carpineti, M.; Ferri, F.; Giglio, M.; Paganini, E.; Perini, U. *Phys. Rev. A* **1990**, *42*, 7347. Piazza, R.; Bellini, T.; Degiorgio, V. *Phys. Rev. Lett.* **1993**, *71*, 4267.
(21) Weitz, D. A.; Huang, J. S.; Lin, M. Y.; Sung, J. *Phys. Rev. Lett.* **1985**, *54*, 1416.
(22) Ying, Q.; Marecek, J.; Chu, B. *J. Chem. Phys.* **1994**, *101*, 2665.
(23) Vailati, A.; Asnaghi, D.; Giglio, M.; Piazza, R. *Phys. Rev. E* **1993**, *48*, R2358. Piazza, R.; Degiorgio, V. *Physica A* **1992**, *182*, 576.
(24) Asnaghi, D.; Carpineti, M.; Giglio, M.; Vailati, A. *Physica A* **1995**, *213*, 148.
(25) Felderhof, B. U.; Jones, R. B. *Phys. Rev. E* **1993**, *48*, 1084. Felderhof, B. U.; Jones, R. B. *Phys. Rev. E* **1993**, *48*, 1142. Felderhof, B. U.; Jones, R. B. *J. Phys.: Condens. Matter* **1994**, *6*, A339.
(26) Doty, P.; Bradbury, J. H.; Holtzer, A. M. *J. Am. Chem. Soc.* **1956**, *78*, 947. Southwick, J. G.; Jamieson, A. M.; Blackwell, J. *Macromolecules* **1981**, *14*, 1728. Rockefort, W. E.; Middleman, S. *J. Rheol.* **1987**, *31*, 337.
(27) Weissenburg, P.; Odijk, T.; Kuil M.; Mandel, M. *Polym. Commun.* **1992**, *33*, 5328.
(28) Wolff, C.; Silberberg, A.; Priel, Z.; Layec-Raphalen, M. N. *Polymer* **1979**, *20*, 281.
(29) Chu, E. Y.; Xu, S. C.; Lee, Z. M.; Sek, C. K. F.; Okamoto, Y.; Pearce, E. M.; Kwei, T. K. *J. Polym. Sci., B: Polym. Phys.* **1995**, *33*, 71.
(30) Horton, J. C.; Donald, A. M. *Polymer* **1991**, *32*, 2418.
(31) Russo, P. S.; Howdhury, A. H.; Mustafa, M. *Mater. Res. Soc. Symp. Proc.* **1989**, *134*, 207. Russo, P. S. In *Reversible Polymeric Gels and Related Topics*; Russo, P. S. ACS Symposium Series 350; American Chemical Society: Washington, DC, 1987; p 1.
(32) Buitenhuis, J.; Dhont, J. K. G.; Lekkerkerker, H. N. W. *Macromolecules* **1994**, *27*, 7267.
(33) Galda, P.; Rehahn, M. *Synthesis* **1996**, 614. Rehahn, M.; Schlüter, A.-D.; Wegner, G. *Makromol. Chem.* **1990**, *91*, 1991. McCarthy, T. F.; Witteler, H.; Pakula, T.; Wegner, G. *Macromolecules* **1995**, *28*, 8350 and references therein. Kallitsis, J. K.; Rehahn, M.; Wegner, G. *Makromol. Chem.* **1992**, *193*, 1021.
(34) Berne, B. J.; Pecora, R. *Dynamic Light Scattering*; Wiley: New York, 1976.
(35) Provencher, S. W. *Comput. Phys. Commun.* **1982**, *27*, 229.
(36) Carpineti, M.; Giglio, M. *Phys. Rev. Lett.* **1993**, *70*, 3828.
(37) Benoit, H.; Doty, P. *J. Phys. Chem.* **1953**, *57*, 958. Benoit, H.; Higgins, J. S. *Polymers and Neutron Scattering*; Clarendon Press: Oxford, U.K., 1994. Schmidt, M. *Macromolecules* **1984**, *17*, 553.
(38) Broesma, S. *J. Chem. Phys.* **1960**, *32*, 1626. Broesma, S. *J. Chem. Phys.* **1981**, *74*, 6989.
(39) Warner, M. *J. Chem. Phys.* **1980**, *73*, 5874; *Phil. Trans. R. Soc., London A* **1993**, *344*, 403.
(40) Schatzel, K. In *Dynamic Light Scattering*; Brown, W., Ed.; Oxford Science Publications: Oxford, U.K., 1993.
(41) Maret, G. In *Mesoscopic Quantum Physics*; Akkermans, E., Montambaux, G., Pichard, J.-L., Zinn-Justin, J., Eds.; Elsevier Science B.V.: Amsterdam, 1995. Weitz, D. A.; Pine, D. J. In *Dynamic Light Scattering*; Brown, W., Ed.; Oxford Science Publications: Oxford, U.K., 1993. Kaplan, P. D.; Yodh, A. G.; Pine, D. J. *Appl. Opt.* **1993**, *32*, 3828. Bicout, D.; Akkermans, E.; Maynard, R. *J. Phys. I* **1991**, *1*, 471.
(42) Hu, C.-M.; Zwanzig, R. *J. Chem. Phys.* **1974**, *60*, 4354. Perrin, F. *J. Phys. Rad.* **1934**, *V*, 497; **1936**, *VII*, 1.
(43) Schaefer, D. W.; Berne, B. J. *Phys. Rev. Lett.* **1972**, *28*, 475.
(44) Petekidis, G.; Weinhold, J. D.; Kumar, S.; Vlassopoulos, D.; Fytas, G. Unpublished results. van der Schoot, P. *J. Phys. Chem.* **1992**, *96*, 6083.

MA961366S